Title: A Carbon Nanotube Optical Rectenna

Authors: Asha Sharma[1,3‡], Virendra Singh[1‡], Thomas L. Bougher[1‡], and Baratunde A. Cola[1,2*]

Affiliations:
[1]George W. Woodruff School of Mechanical Engineering, Georgia Institute of Technology, Atlanta, Georgia 30332, USA.
[2]School of Materials Science and Engineering, Georgia Institute of Technology, Atlanta, Georgia 30332, USA.
[3]Center for Organic Photonics and Electronics, School of Electrical & Computer Engineering, Georgia Institute of Technology, Atlanta, Georgia, 30332, USA.
*Correspondence to: cola@gatech.edu
‡These authors contributed equally

An optical rectenna – that is, a device that directly converts free-propagating electromagnetic waves at optical frequencies to d.c. electricity – was first proposed[1] over 40 years ago, yet this concept has not been demonstrated experimentally due to fabrication challenges at the nanoscale.[2,3] Realizing an optical rectenna requires that an antenna be coupled to a diode that operates on the order of 1 petahertz (switching speed on the order of a femtosecond). Ultralow capacitance, on the order of a few attofarads,[3,4] enables a diode to operate at these frequencies; and the development of metal-insulator-metal tunnel junctions with nanoscale dimensions has emerged as a potential path to diodes with ultralow capacitance,[2,3] but these structures remain extremely difficult to fabricate and couple to a nanoscale antenna reliably.[2] Here we demonstrate an optical rectenna by engineering metal-insulator-metal tunnel diodes, with ultralow junction capacitance of approximately 2 attofarads, at the tips of multiwall carbon nanotubes, which act as the antenna[5,6] and metallic electron field emitter in the diode. This demonstration is achieved using very small diode areas based on the diameter of a single carbon nanotube (about 10 nanometers), geometric field enhancement at the carbon nanotube tips, and a low work function semi-transparent top metal contact. Using vertically-aligned arrays of the diodes, we measure d.c. open-circuit voltage and short-circuit current at visible and infrared electromagnetic frequencies that is likely due to a rectification process, and quantify minor contributions from thermal effects. In contrast to recent reports of photodetection based on hot electron decay in plasmonic nanoscale antenna,[7,8] a coherent optical antenna field appears to be rectified directly in our devices, consistent with rectenna theory.[4,9,10] Our devices show evidence of photon-assisted tunneling[9,10] that reduces diode resistance by two orders of magnitude under monochromatic illumination. Additionally, power rectification is observed under simulated solar illumination. Numerous current-voltage scans on different devices, and between 5-77 degrees Celsius, show no detectable change in diode performance, indicating a potential for robust operation.

A rectenna operates by coupling electromagnetic energy into an oscillating voltage and current (that is, a.c. electricity) in an antenna. The diode coupled to the antenna then rectifies the a.c. current to produce d.c. electricity output that can be coupled to a load to produce usable energy. This process utilizes the wave nature of light in contrast to traditional semiconductor

photovoltaics, which rely on the particle nature of light. The historical barrier to creating an optical rectenna has been creating a diode that is fast enough to switch at optical frequencies (greater than 430 THz), with the only previous evidence for optical rectification occurring in experiments that establish a vacuum gap between nanoscale metals.[11,12] Using extremely high illumination intensity (22.6 kW/cm²) in a plasmonic nanoscale vacuum gap,[12] Ward et al. recently reported optical rectification photocurrent of ~ 8 nA and an inferred optical voltage of ~ 30 mV, providing strong evidence that a solid-state optical rectenna may be possible if an appropriate diode is developed.

Single-frequency energy conversion efficiency greater than 90 percent has been demonstrated[13] for rectification devices operating at much lower frequencies in the microwave spectrum (~ 2 GHz). Theory suggests[9,10] that efficiencies this high could also be achieved for optical rectification using an ideal diode – that is, one with ultralow capacitance and resistance, and high non-linearity and asymmetry. The cutoff frequency for a rectenna is defined[4] as $f_c = 1/(2\pi \cdot R_A \cdot C_D)$ when diode resistance is much greater than antenna resistance, where R_A is the antenna resistance and C_D is the capacitance of the rectenna diode. This assumption is likely appropriate for nanoscale rectenna because, while a number of efficient designs for optical antennas exist,[14] contact and quantum resistances are typically large in nanoscale devices.[15] Because the diode capacitance is[4] $C_D = \varepsilon_0 \varepsilon . A/d$, where ε_0 is permittivity of vacuum, ε relative permittivity of insulator, A area, and d insulator thickness, reducing the diode area is a simple approach to increase cutoff frequency and enable optical rectification. Metal-insulator-metal (M-I-M) diodes are quantum mechanical tunneling devices, with fundamental operating speeds on the order of a femtosecond, that are capable of rectification at optical frequencies if they can be fabricated with proper nanoscale dimensions.[3] A natural approach for efficient antenna-diode coupling is to use one electrode in the M-I-M diode as the antenna. Multiwall carbon nanotubes (MWCNTs) exhibit antenna like interaction with light,[5,6] and are well established as low-resistance metallic electrical conductors[16,17] that can be synthesized as dense vertical arrays with controlled lengths and diameters. Here, we engineer and experimentally demonstrate an optical rectenna (Fig. 1a) by exploiting these unique features, the very small diameters of nanotubes, and the ability to build M-I-M diodes with nanoscale precision and the required ultralow capacitance. We leverage the fact that vertically aligned CNT arrays can create a high number density of rectennas connected in parallel to overcome the small current at each nanoscale diode.

Carbon nanotubes (CNTs) are hollow nanoscale filaments composed of a single sheet of carbon atoms (single-wall CNTs), or several concentric sheets of carbon atoms (MWCNTs), and have exceptional electrical[16,17] and optical properties.[18,19] For example, CNTs can be used to absorb electromagnetic radiation in essentially the entire electromagnetic spectrum due to both free carrier (intraband) and excitonic (interband) absorption processes,[18-20] which, when combined with high carrier mobilities, makes them especially suited for broadband photonic and optoelectronic applications.[21,22] In contrast to single-wall CNTs, which can be semiconducting or metallic based on their chirality, MWCNTs exhibit metallic properties[17] due to the presence of at least one metallic chirality, and do not typically show an excitonic photovoltaic effect.[20] The photoresponse of metallic CNTs is usually caused by thermal effects;[20] however, the ability of metallic CNTs to behave as antennae,[5,6] coupled with their small tip area, make theses materials ideal candidates for a combined antenna-rectifying diode (that is, a rectenna).

Vertically aligned arrays (density ~ 10^{10}/cm^2 and height ~ 10 μm) of MWCNTs (8-10 nm in diameter) were grown by chemical vapor deposition (Methods), and MWCNT-I-M tunnel diodes were fabricated at the nanotube tips using atomic layer deposition of Al$_2$O$_3$ (8 nm in thickness –

Fig. 1b and 1c) and thermal evaporation of a low work function top metal electrode (Fig. 1b) – a semi-transparent film of Ca (2.9 eV work function) capped by Al (Methods). Our device structure (MWCNT-Al_2O_3-Ca) is analogous to numerous metal whisker point contact diodes[4,23] connected in parallel because the MWCNTs are vertically aligned, physically isolated from each other by the conformal Al_2O_3 coating (Fig. 1b and 1c), and connected to an approximately planar top metal contact film (Fig. 1b). An insulator typically needs to be less than about 2 nm to allow significant electron tunneling and rectification;[24] however, the intrinsic electric field (that is, the field due to asymmetric metal work functions) is enhanced (Fig. 2a) at the MWCNT tips in our device geometry, similar to field enhancement that occurs in CNT field emitters,[25] which produces an estimated effective insulating barrier thickness of 1.5 nm for a deposited Al_2O_3 thickness of 8 nm (Figs. S1-S4). We note that the actually atomic interfaces may be separated by a distance smaller than 8 nm due to diffusion of top metal atoms into the oxide during deposition (Fig. S4 shows an effective insulating barrier thickness of 2.8 nm for a deposited Al_2O_3 thickness of 8 nm in a planar device with similar contrast in work function). The rectification asymmetry is also enhanced (Fig. S5) and turn-on voltage decreased (Fig. 2b and Fig. S1) by the large difference in work function between MWCNTs (5 eV work function, Fig. S6) and Ca. The MWCNT-Al_2O_3-Ca diode has a work function difference of 2.1 eV while the diode with an Al (4.3 eV work function) top metal has a work function difference of only 0.7 eV. We note that devices with Al top metal contact did not produce a detectable photoresponse in our testing due to their high turn-on voltages.

Since electron transport is most efficient in the axial direction of MWCNTs,[16,17] the diode area where electron tunneling occurs is likely defined by the outer MWCNT tip diameter of 8-10 nm as illustrated in Fig. 1a. Thus, diode capacitance is inherently on the order of a few attofarads in our design, which enables operation at petahertz frequencies. To confirm this, specific capacitances on the order of 3±0.6 $\mu F/cm^2$ for entire devices, or approximately 2 attofarads per MWCNT junction, are extracted from capacitance measurements in a standard low frequency range (Fig. 2c) by using the number density of MWCNTs ($\sim 10^{10}/cm^2$) to determine the real or active device area, which is about 200 times smaller than the apparent device area. From the capacitance measurements we estimate a relative permittivity of 3.8 for the Al_2O_3 layer, which agrees with reports for atomic layer deposited Al_2O_3 in this thickness range[26] (Supplementary Information section S3, Fig. S7). The inset in Fig. 2c shows that capacitance of the MWCNT-I-M diodes is stable from at least -2 to 2 V, which is important for robust device operation. While thicker oxide produces lower capacitance (Fig. 2c), this is not a viable approach to increase the device cutoff frequency because of the associated increase in resistance, which diminishes current and nonlinearity in the diode (Fig. 2d and Fig. S8). The current-voltage characteristics, $I(V_{dc})$, of our MWCNT-I-M diodes show rectified currents up to 2 A cm^{-2} at less than 1 V applied bias (Fig. 2b), and are consistent over numerous scans on the same device and for several different devices created from similar MWCNT arrays (Fig. 2b and Fig. S9). In addition, the current-voltage characteristics show little temperature dependence from 5 to 77 ˚C (Fig. 2e), indicating that there are no detectable effects from thermal expansion in our devices, and that our devices do not behave as semiconductor based diodes or semiconducting CNT Schottky junctions, which are known to have strong temperature dependence.[27]

Our MWCNT rectenna devices are illuminated using lasers with wavelengths of 1064 nm (282 THz, 92 mW cm^{-2}) and 532 nm (564 THz, 26 mW cm^{-2}), and an AM 1.5 solar simulation source (100 mW cm^{-2}). Our MWCNT arrays are $\sim$ 10 μm in height, which is much longer than the wavelengths of illumination, so they respond as antenna in the resistive limit[4] rather than

being resonant at the test frequencies. Measurements are performed at room temperature and the details of the optical and electrical measurements are described in the Methods. While the asymmetry in our MWCNT-Al$_2$O$_3$-Ca tunnel junctions could produce significant thermal voltages,[28] we do not expect this in our testing where illumination is diffused over centimeter-size areas, and about 10,000 times less intense than intensities used in a prior optical rectification study.[12] The maximum photon energy in our tests is below the energy required to sustain excited electrons in the conduction band of amorphous AlO$_x$,[29] which is required to produce significant photocurrent based on hot-electron transport in M-I-M diodes.[30,31]

Classically, rectification can be identified from examining the nonlinearity of diode conductance,[28] where the amplitude of a small applied a.c. voltage bias, $V_{ac} \cos(\omega t)$, can be related to the rectified d.c. current as[12] $I \approx [I(V_{dc}) + 1/2 \, (\beta/R)V_{ac}^2]$, where $\beta = 1/2 \, (\partial^2 I/\partial V^2)/(\partial I/\partial V)$ is the diode responsivity and $R = 1/(\partial I/\partial V)$ is the diode differential resistance. However, when a nanoscale junction is illuminated with radiation of energy $\hbar\omega$, the plasmonic response of the junction produces an a.c. voltage, V_{opt}, at frequency ω across the junction, and, in the limit of small a.c. amplitudes ($eV_{opt} \ll \hbar\omega$), a quantum correction is required to consider photon-assisted tunneling.[9] In this semi-classical picture,[9] the diode differential resistance is

$$R_{qc} = \frac{(2\hbar\omega/e)}{[I(V_{dc}+\hbar\omega/e)-I(V_{dc}-\hbar\omega/e)]}, (1)$$

and the diode responsivity is

$$\beta_{qc} = \frac{e}{\hbar\omega} \frac{[I(V_{dc}+\hbar\omega/e)-2I(V_{dc})+I(V_{dc}-\hbar\omega/e)]}{[I(V_{dc}+\hbar\omega/e)-I(V_{dc}-\hbar\omega/e)]}, (2)$$

where $= R_{qc}$, $\beta = \beta_{qc}$, and $V_{opt} = V_{ac}$ as $\hbar\omega \to 0$. The semi-classical rectified d.c. current can be expressed as $I = [I(V_{dc}) + 1/2 \, (\beta_{qc}/R_{qc})V_{opt}^2]$, and the semi-classical rectified d.c. diode voltage as $V_D = -1/2 \, \beta_{qc}V_{opt}^2$, which is valid when the rectenna is operating below its cutoff frequency.[4] Power generation, P_{out}, can be expressed as one-half the open-circuit voltage (V_{oc}) times one-half the short-circuit current (I_{sc}), which, in terms of basic device parameters is

$$P_{out} = -\beta_{qc}^2 V_{opt}^4 / 16R_{qc}, (3)$$

where β_{qc} and R_{qc} are at zero-bias conditions ($V_{dc} = 0$). The maximum responsivity and optical voltage at unity quantum efficiency[9] are $e/\hbar\omega$ and $\hbar\omega/e$, respectively, which reduces equation (3) to $P_{out} = -(\hbar\omega/e)^2/16R_{qc}$.

Our MWCNT rectenna devices show increased nonlinearity and reduced zero-bias differential resistance when illuminated with 1064 nm, 532 nm, and AM 1.5 solar light (Fig. 3 and Fig. S10), in agreement with expectations based on photon-assisted tunneling and equations (1) and (2). For example, at $V_{dc} = 0$, $R_{qc} = 70$ ohm-cm^2 and $\beta_{qc} = 0.4$ V^{-1} for 1064 nm illumination (Fig. 3a), and these results are consistent with the values in Table S1, which are based on applying a classical treatment to the illuminated $I(V_{dc})$ curve (Fig. S11 and Table S1). The photoresponse (photocurrent divided by illumination power) of our devices (Fig. 3a) to 532 nm light is higher than the response to 1064 nm light (5 A/W for 532 nm and 1.4 A/W for 1064 nm, at 1.25 V), which also agrees with expectations based on photon-assisted tunneling. The photoresponse of our devices is at least 6 orders of magnitude higher than in prior optical rectification studies (Table S2). We note that, in contrast to the photocurrent response, the open-circuit photovoltage response to 532 nm light is lower than the response to 1064 nm light (Fig. 3b and c), which we discuss further below as evidence for rectenna operation. Our devices generate power in the second quadrant of the $I(V_{dc})$ curve, as expected[9,12] in an optical rectification photoresponse. This highlights the different physics in our devices compared with

4

the photovoltaic effect induced by the bandgap in semiconductors, which is known to generate power in the fourth quadrant of the device $I(V_{dc})$ curve. The measured V_{oc} and I_{sc} (Table S1) agree reasonably well with the values extracted from the $I(V_{dc})$ curves in Fig. 3. The I_{sc} of our MWCNT rectenna devices (Table S1) is about 10 times smaller for broadband solar illumination compared to monochromatic illumination, which could be caused by frequency mixing losses under broadband illumination.[10] This is consistent with the higher zero-bias resistance under solar illumination (Fig. 3d inset) compared to laser illumination (Fig. 3b and 3c insets).

Thermal effects can hamper clear identification of a rectification photoresponse.[28] To isolate possible thermoelectric effects in CNTs[21,22] on the measured photoresponse of our devices, we modified our devices with an opaque Al capping layer (150 nm thick), to prevent an optical rectification response, and heated them with a 532 nm laser intensity of 11.2 W cm^{-2}, about 112 times more intense than the maximum intensity in our rectenna response tests. The magnitude and sign of the measured voltage changes with the position of the heating spot with respect to the contacts (Fig. S12), consistent with a thermoelectric effect.[21,22] The maximum thermoelectric response based on 112 times higher illumination intensity is less than 1% of the measured optical rectification V_{oc} for 1064 nm, 532 nm, and solar illumination (Fig. 4a). The distance between contacts in our vertical device architecture ($\sim$ 10 μm) is much smaller than those used in horizontally-aligned CNT photodetectors based on the thermoelectric effect ($\sim$ 1 mm),[22] which makes it difficult to support a significant temperature gradient at illumination intensities $\sim$ 100 mW cm^{-2}. Additionally, the change in nonlinearity in the $I(V_{dc})$ curves for our devices (Fig. 3) is not observed in a thermoelectric response[21,22] where the $I(V_{dc})$ curve remains linear under illumination.

Using diode characteristics extracted from the illuminated $I(V_{dc})$ curves as discussed above, the change in diode responsivity with voltage is shown in Fig. 4b for the same device under 1064 nm and 532 nm laser illumination. The decrease in responsivity with monochromatic illumination compared to the dark diode characteristics could be the result of photo-excited electrons tunneling with higher probability under reverse bias (Fig. 2a), due to the much higher carrier concentration in metals compared to MWCNTs. There is minor change in the responsivity under solar illumination compared to dark conditions, except near the zero-bias condition where there is a significant decrease (Table S1). Using the zero-bias responsivity under illumination to normalize V_{oc}, the voltage response to 1064 nm illumination on the same device appears to scale linearly with illumination power, and intercepts the origin (Fig. 4c) as expected. This normalization is equivalent to V_{opt}^2, which is proportional to the power received by the MWCNT antenna.[4] Additionally, the measured V_{oc} is polarization dependent (Fig. 4c inset), which is consistent with the MWCNTs behaving as classical antenna.[5,6] The results in Fig. 4 indicate that despite the slightly higher illumination power, the optical voltage under solar illumination is significantly less than the optical voltage under 1064 nm laser illumination, and that larger photon energy does not necessarily produce a larger optical voltage without consideration of illumination power, and likely the degree of illumination coherence. These finding appear to agree qualitatively with the rectenna V_{oc} predicted by a recent thermodynamic analysis.[32] Additionally, the $\partial^2 I/\partial V^2$ computed from the illuminated $I(V_{dc})$ curve, to approximate the required quantum correction, is directly proportional to photocurrent in our devices (Fig. S13), which is additional evidence for the optical rectification mechanism.[12]

The inferred V_{opt} for solar, 1064 nm, and 532 nm illumination are 52, 68, and 33 mV, respectively (Fig. 3 devices). These optical voltages are on the same order as the optical voltages inferred from rectification in a symmetric gold vacuum tunnel junction under 10,000 times

greater illumination intensity,[12] which suggests that the optical coupling to our MWCNT antenna could be more efficient due to collective antenna coupling in the arrays.[5,6] However, further experimental and theoretical work is required to fully understand the generation and rectification of optical voltage in MWCNT arrays, and to characterize the effective antenna resistance. These studies are required to estimate an efficiency limit – based on equation (3) – and a precise cutoff frequency for our rectenna devices. Our results, however, demonstrate operation at 564 THz, which is supported by the extremely low capacitance of our diodes (~ 2 attofarads, which using a conservative antenna resistance estimate of 100 Ω, the range of values for a single metal whisker antenna[4] with no enhancement from collective effects as in our devices, gives a cutoff frequency of ~ 800 THz). Considering the number density of MWCNTs in the arrays (~ 10^{10}/cm^2), the resistance of a single MWCNT-I-M junction is on the order of 1 TΩ, which is several orders of magnitude higher than the resistance of typical MWCNT interconnects.[15] Our device junction resistances are higher because they include the intrinsic resistance of the oxide-coated MWCNT and contact resistances, and the resistance of the oxide barrier, which increases exponentially with the oxide thickness in a tunnel diode.[24] The high electrical resistance of a single MWCNT-I-M junction likely creates poor impedance matching with the MWCNT antenna, which limits the rectified power in a single junction[3] and is a major issue to focus on for future improvements. The large number density of MWCNT-I-M diodes connected in parallel, however, increases current and power production at the device level substantially. The measured power conversion efficiency of our MWCNT array rectenna device is about 10^{-5} percent under 1064 nm laser illumination (Table S1), which is the highest efficiency measured in our present devices. However, this conversion efficiency appears to be limited by the quality and geometry of our CNTs and other fabrication challenges rather than predicted fundamental limits,[9,10] and could be increased dramatically with more efficient optical voltage coupling, thinner insulator barriers, and low-resistance electrical contacts to the MWCNTs. Achieving these improvements to our device could enable definitive evidence of the optical rectenna mechanism as well as practical applications.

METHODS

Device fabrication. Vertically-aligned arrays of multiwall carbon nanotubes (MWCNTs) were grown on Si substrates using a low-pressure chemical vapor deposition (LPCVD) process at 850 °C and 1 kPa in an Aixtron Black Magic$^©$ reactor with C_2H_2 as the carbon source gas. Ti, Al, and Fe films with thicknesses of 100, 10, and 3 nm were evaporated onto the Si as support as catalyst layers for MWCNT growth. To allow probing away from the active area of the devices, a SiO_x barrier layer (250 nm) was deposited on half of the Si substrate (Fig. 1a). The growth time was between 1 to 3 minutes to produce MWCNTs with average heights of ~ 10 μm. Scanning and transmission electron microscopy were used to characterize the structure of MWCNTs and their coatings. The average diameters of the MWCNTs are approximately 8-10 nm and the average number of walls is 6 (Fig. 1c). Al_2O_3 dielectric layers of 8, 12, or 15 nm were deposited on the MWCNTs by atomic layer deposition (ALD) at 250 °C using trimethylaluminum (TMA) and water (H_2O) vapors. These thicknesses are based on optimized ALD cycles (100 cycles = 10 nm), which were calibrated on planar Si substrates. Purge times of 30 seconds were used in each ALD cycle for both TMA and H_2O to enable TMA and H_2O vapor to diffuse completely from the MWCNT tips to the substrate base. In between two sets of ALD, oxygen plasma was used to oxidize the surface of the MWCNTs and introduce hydrophilic moieties[16,17] (-OH and -COOH),

which promotes uniform nucleation (Fig. 1b and 1c) and conformal deposition of Al_2O_3 on the MWCNTs. A metal top contact of Ca (40 nm)/Al (20 nm), or 100 nm Al for the device in Fig. 2b and 2e, was then vacuum (base pressure less than 10^{-7} torr) deposited on the arrays using a shadow mask to form the MWCNT rectenna devices. The source metals were from Lesker and purity of 99% or greater. The Al layer is required to prevent or minimize oxidation of Ca in air.

Electrical measurements. The current-voltage $I(V_{dc})$ characteristics of MWCNT-I-M rectenna were measured using an Agilent E5272A source monitor unit connected to a DC electrical probing station with a temperature-controlled stage. The resistance of the probe and lead wires is on the order of 1 Ω. Capacitance-frequency characteristics were measured using HP 4284 capacitance meter at room temperature. The capacitance, and the operating electric field strength limits in MWCNT-I-M devices were established by measuring specific capacitances as a function of DC bias for oxide thicknesses of 8 and 15 nm at a frequency of 10^5 Hz and 20 mV$_{rms}$. The work functions of MWCNTs were measured in air using a Kelvin probe (Besocke Delta Phi) with reference to a highly ordered pyrolytic graphite (HOPG) crystal sample. Electrical and optical tests were performed in a glove box under a nitrogen environment, and at near atmospheric pressure and temperature, except for the temperature dependent current-voltage scans.

Optical measurements. An infrared (IR) continuous waveform laser with 1064 nm wavelength (282 THz) at intensities of 92 mW cm^{-2} and 243 mW cm^{-2}; green continuous waveform laser with 532 nm wavelength (564 THz) at an intensity of 26 mW cm^{-2}; and AM 1.5 solar simulation source at an intensity of 100 mW cm^{-2} were used to test rectenna response. The angle of illumination was aligned to the surface normal, except in measurements as a function of polarization as discussed below. The estimated transmissivity of the top metal contact (40 nm Ca/20 nm Al) for the tested wavelengths is 10% based on measurements with the same contact film composition on a transparent substrate. The polarization of the IR laser (the output is linearly polarized) was controlled using a half waveplate, and a linear polarizer. The open circuit voltage response as a function of polarization was measured by rotating polarization angle of the laser beam with respect to the MWCNT antenna alignment, and aligning the illumination at 45 degrees from the surface normal. All measurements were performed at room temperature.

References:
1   Bailey, R. L. A proposed new concept for a solar-energy converter. *J. Eng. Power* **94**, 73-77 (1972).
2   Donchev, E. *et al.* The rectenna device: From theory to practice (a review). *MRS Energy & Sustainability: A Review Journal* **1**, 1-34 (2014).
3   Moddel, G. & Grover, S. *Rectenna Solar Cells*. (Springer New York, 2013).
4   Sanchez, A., Davis, J. C. F., Liu, K. C. & Javan, A. The MOM tunneling diode: Theoretical estimate of its performance at microwave and infrared frequencies. *J. Appl. Phys.* **49**, 5270-5277 (1978).
5   Wang, Y. *et al.* Receiving and transmitting light-like radio waves: Antenna effect in arrays of aligned carbon nanotubes. *Appl. Phys. Lett.* **85**, 2607-2609 (2004).

6   Kempa, K. *et al.* Carbon Nanotubes as Optical Antennae. *Adv.d Mater.* **19**, 421-426 (2007).

7   Knight, M. W., Sobhani, H., Nordlander, P. & Halas, N. J. Photodetection with Active Optical Antennas. *Science* **332**, 702-704 (2011).

8   Giugni, A. *et al.* Hot-electron nanoscopy using adiabatic compression of surface plasmons. *Nature Nanotech.* **8**, 845-852 (2013).

9   Sachit, G., Saumil, J. & Garret, M. Quantum theory of operation for rectenna solar cells. *J. Phys. D: Appl. Phys.* **46**, 135106 (2013).

10   Joshi, S. & Moddel, G. Efficiency limits of rectenna solar cells: Theory of broadband photon-assisted tunneling. *Appl. Phys. Lett.* **102**, 083901-083905 (2013).

11   Nguyen, H. Q. *et al.* Mechanisms of current rectification in an STM tunnel junction and the measurement of an operational tunneling time. *IEEE Trans. Elec. Dev.* **36**, 2671-2678 (1989).

12   Ward, D. R., Huser, F., Pauly, F., Cuevas, J. C. & Natelson, D. Optical rectification and field enhancement in a plasmonic nanogap. *Nature Nanotech.* **5**, 732-736 (2010).

13   Brown, W. C. Optimization of the Efficiency and Other Properties of the Rectenna Element. *Microwave Symposium, 1976 IEEE-MTT-S International,* 142-144 (1976).

14   Novotny, L. & van Hulst, N. Antennas for light. *Nature Photon.* **5**, 83-90 (2011).

15   Songkil, K. *et al.* Fabrication of an UltraLow-Resistance Ohmic Contact to MWCNT-Metal Interconnect Using Graphitic Carbon by Electron Beam-Induced Deposition (EBID). *IEEE Trans. Nanotech.* **11**, 1223-1230 (2012).

16   Ebbesen, T. W. *et al.* Electrical conductivity of individual carbon nanotubes. *Nature* **382**, 54-56 (1996).

17   Frank, S., Poncharal, P., Wang, Z. L. & de Heer, W. A. Carbon Nanotube Quantum Resistors. *Science* **280**, 1744-1746 (1998).

18   Avouris, P., Freitag, M. & Perebeinos, V. Carbon-nanotube photonics and optoelectronics. *Nature Photon.* **2**, 341-350 (2008).

19   Nanot, S., Hároz, E. H., Kim, J.-H., Hauge, R. H. & Kono, J. Optoelectronic Properties of Single-Wall Carbon Nanotubes. *Adv. Mater.* **24**, 4977-4994 (2012).

20   Barkelid, M. & Zwiller, V. Photocurrent generation in semiconducting and metallic carbon nanotubes. *Nature Photon.* **8**, 47-51 (2014).

21   Nanot, S. *et al.* Broadband, Polarization-Sensitive Photodetector Based on Optically-Thick Films of Macroscopically Long, Dense, and Aligned Carbon Nanotubes. *Sci. Rep.* **3**, 1335 (2013).

22   He, X. *et al.* Carbon Nanotube Terahertz Detector. *Nano Letters* **14**, 3953-3958 (2014).

23   Daneu, V., Sokoloff, D., Sanchez, A. & Javan, A. Extension of Laser Harmonic-Frequency Mixing Techniques into 9 μ Region with an Infrared Metal-Metal Point-Contact Diode. *Appl. Phys. Lett.* **15**, 398-401 (1969).

24   Simmons, J. G. Electric tunnel effect between dissimilar electrodes separated by a thin insulating film. *J. Appl. Phys.* **34**, 2581-2590 (1963).

25   Xu, X. & Brandes, G. A method for fabricating large-area, patterned, carbon nanotube field emitters. *Appl. Phys. Lett.* **74**, 2549-2551 (1999).

26   de Heer, W. A., Châtelain, A. & Ugarte, D. A Carbon Nanotube Field-Emission Electron Source. *Science* **270**, 1179-1180 (1995).

27   Appenzeller, J., Radosavljević, M., Knoch, J. & Avouris, P. Tunneling Versus Thermionic Emission in One-Dimensional Semiconductors. *Phys. Rev. Lett.* **92**, 048301 (2004).

28   Tu, X. W., Lee, J. H. & Ho, W. Atomic-scale rectification at microwave frequency. *J. of Chem. Phys.* **124**, 021105 (2006).

29   Kovacs, D. A., Winter, J., Meyer, S., Wucher, A. & Diesing, D. Photo and particle induced transport of excited carriers in thin film tunnel junctions. *Phys. Rev. B* **76**, 235408 (2007).

30   Chalabi, H., Schoen, D. & Brongersma, M. L. Hot-Electron Photodetection with a Plasmonic Nanostripe Antenna. *Nano Lett.* **14**, 1374-1380 (2014).

31   Wang, F. & Melosh, N. A. Plasmonic Energy Collection through Hot Carrier Extraction. *Nano Lett.* **11**, 5426-5430 (2011).

32   Lerner, P. B., Miskovsky, N. M., Cutler, P. H., Mayer, A. & Chung, M. S. Thermodynamic analysis of high frequency rectifying devices: Determination of the efficiency and other performance parameters. *Nano Energy* **2**, 368-376 (2013).

Author Contributions: B.A.C. conceived the rectenna device and wrote the manuscript with comments and edits from all authors. A.S. and V.S. fabricated the devices and characterized materials. A.S. measured rectenna response on all devices. T.L.B performed the device modeling and thermoelectric response experiments. All authors contributed to data analysis and interpretation.

Additional information: Supplementary information accompanies this paper at www.nature.com/. Reprints and permission information is available online at http://npg.nature.com/reprintsandpermissions/. Correspondence and requests for materials should be addressed to B.A.C.

Competing financial interests: Georgia Tech has applied for a patent, application no. PCT/US2013/065918, related to the design methods and materials produced in this work.
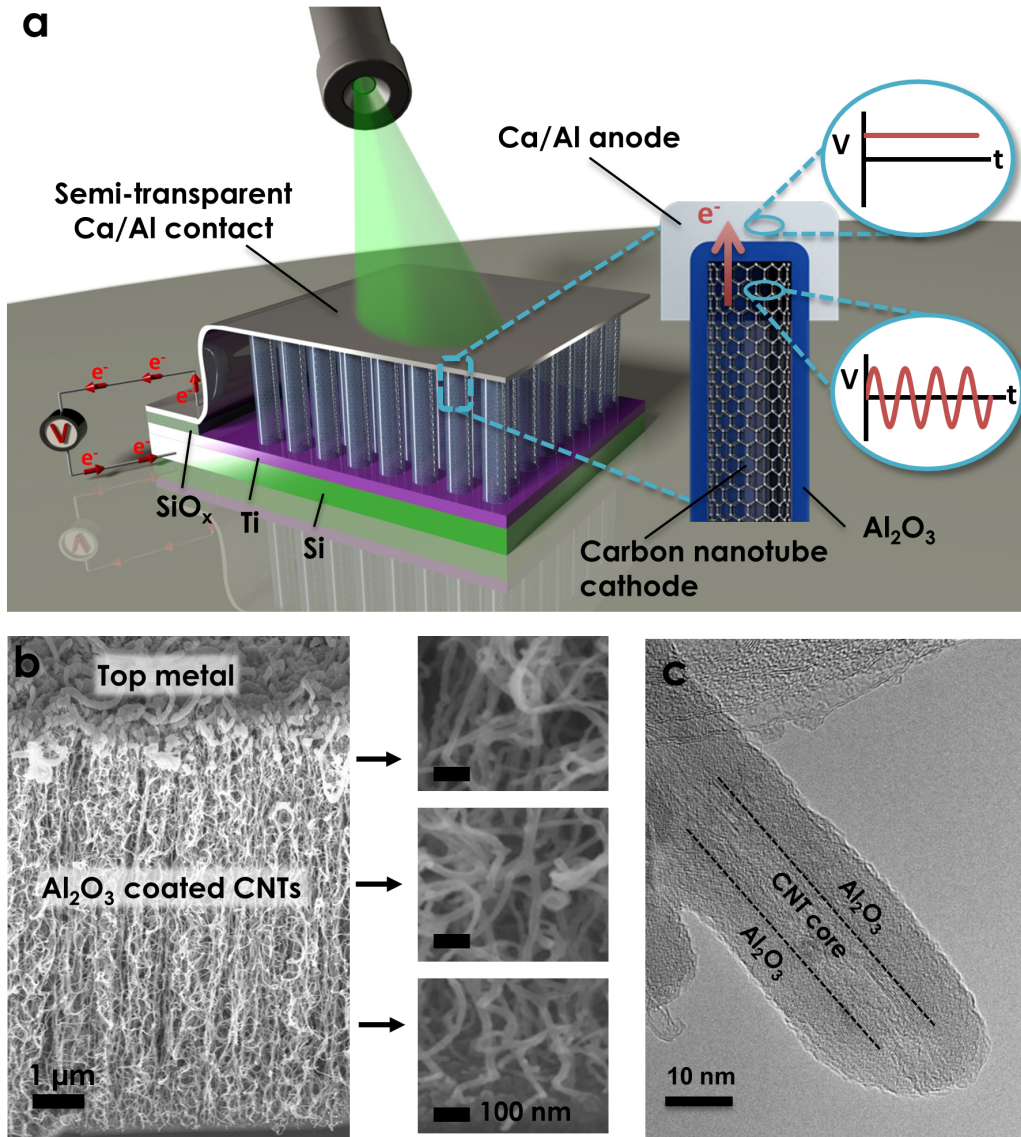
Figure 1| Carbon nanotube optical rectification device. a, Schematic of the vertically-aligned multiwall carbon nanotube-insulator-metal (MWCNT-I-M) optical rectification device. The effective diode structure at the tip of a single MWCNT is shown to the right. The blowouts show an a.c. input signal in the MWCNT antenna, and a d.c. output signal in the top metal anode. **b,** A scanning electron micrograph (SEM) of a representative MWCNT-I-M device. The images to the right show blowouts of the bottom, middle, and top region of the oxide-coated MWCNTs (each scale bar is 100 nm). **c**, A transmission electron micrograph (TEM) of a representative oxide-coated MWCNT. The dotted black lines show the interface of the MWCNT and oxide coating.
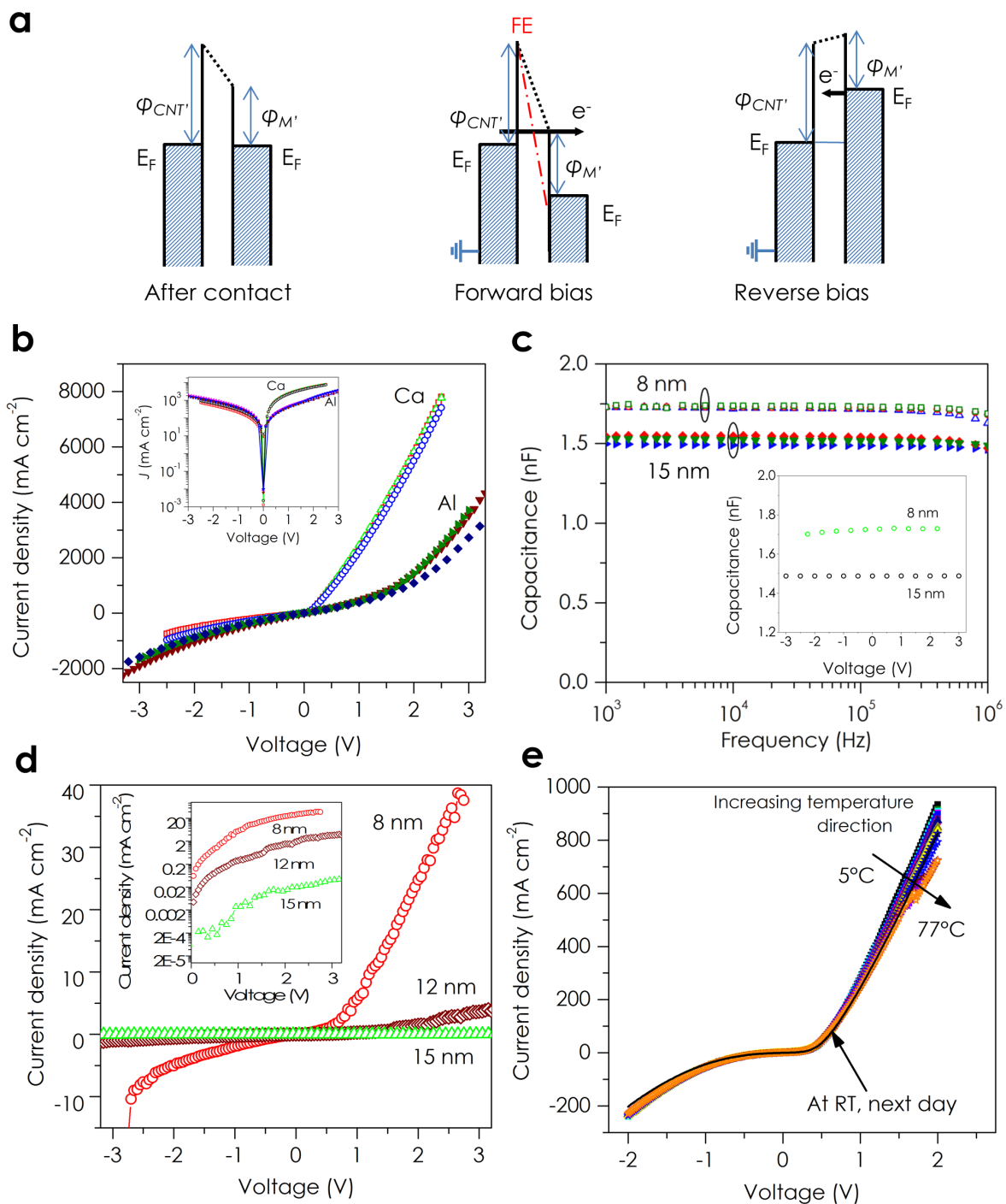
Figure 2| Carbon nanotube-insulator-metal tunnel diode characteristics. a, An approximate potential energy level diagram for an asymmetric tunnel diode with MWCNT-I-M structure. The dash-dot red line shows the reduced effective barrier thickness due to geometric field enhancement in the diode at MWCNT tips. The Fermi level is denoted as E_F, and ϕ is work function (subscripts "CNT" and "M" are for MWCNT and metal, respectively). The flow of electrons near the Fermi level is denoted by the direction of the arrow and ē. **b,** Comparison of the current-voltage characteristics of MWCNT-I-M vertical diode array devices using lower work function metal (Ca), and higher work function metal (Al) (the inset shows semi-logarithmic plots of the data, where

J is current density).   **c,** Capacitance (*C*) (device area = 0.1 cm^2) of MWCNT-I-M (MWCNT-Al$_2$O$_3$-Ca) structures using 8 nm and 15 nm of Al$_2$O$_3$ as a function of frequency at 20 mV$_{rms}$. The inset shows the voltage stability of the devices. **d,** The current-voltage characteristics of the tunnel diodes using 8, 12, and 15 nm of Al$_2$O$_3$ (the inset shows semi-logarithmic plots of the data). **e,** Temperature dependent current-voltage characteristics of MWCNT-I-M devices between 5-77 ˚C with an increment of ~ 5 ˚C. The devices were tested again at room temperature the next day. The devices in b, d, and e are from different MWCNT batches with variations in resistances and current densities.
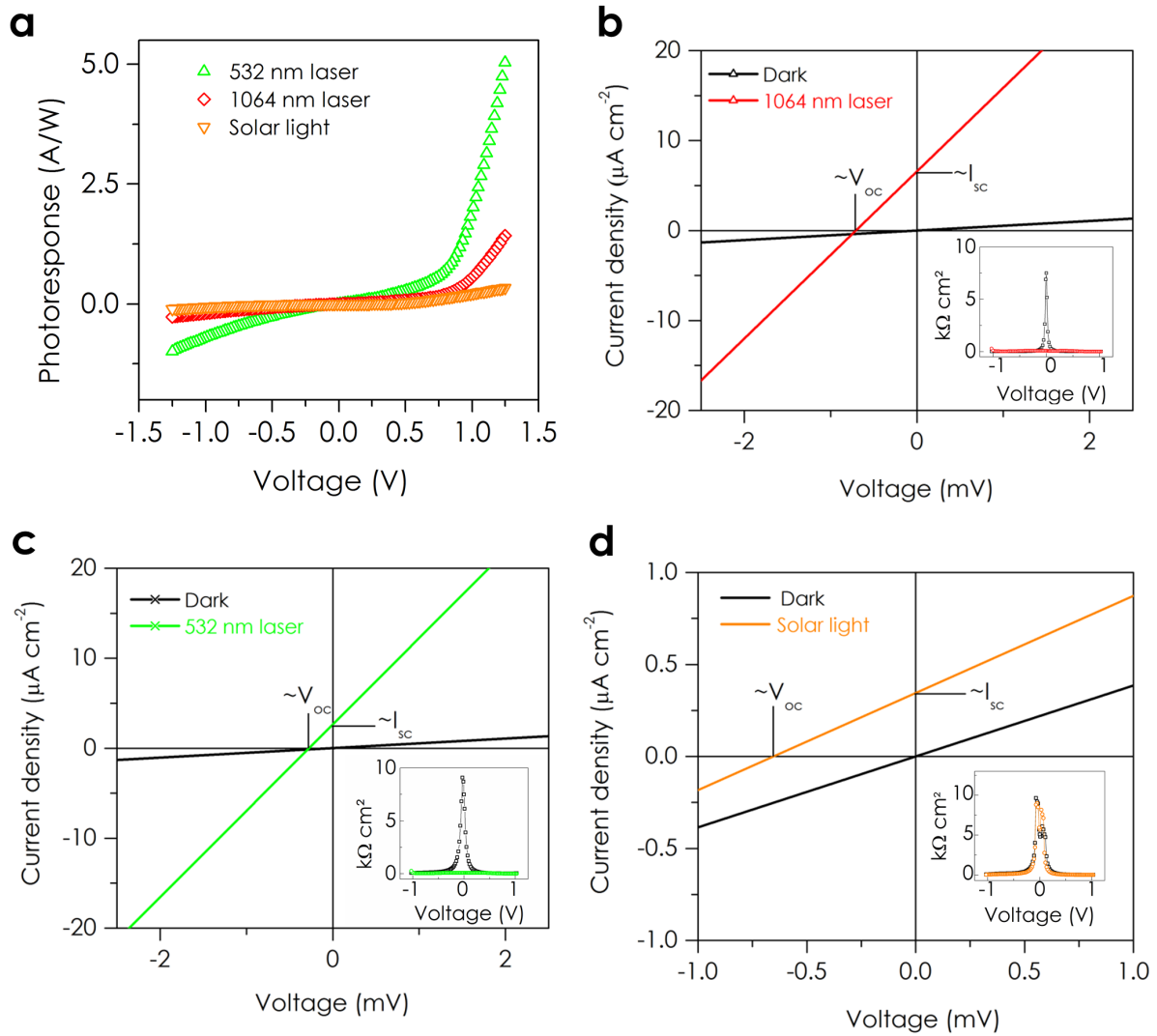
Figure 3| Optical rectification of infrared, visible, and simulated solar light. a, Photoresponse (photocurrent divided by illumination power) versus voltage of device responding to 1.5 AM solar (100 mW cm^{-2}), 1064 nm (92 mW cm^{-2}), and 532 nm (26 mW cm^{-2}) illumination with 10% transmission through the top metal contact. **b**, **c**, and **d** show high-resolution views of the illuminated current-voltage response to 1064 nm laser, 532 nm laser, and 1.5 AM solar illumination, respectively. The V_{oc} and I_{sc} noted in the high-resolution views of the current-voltage responses are the measured open circuit voltage and short circuit current for each illumination case. The insets in **b**, **c**, and **d** are the differential resistances.
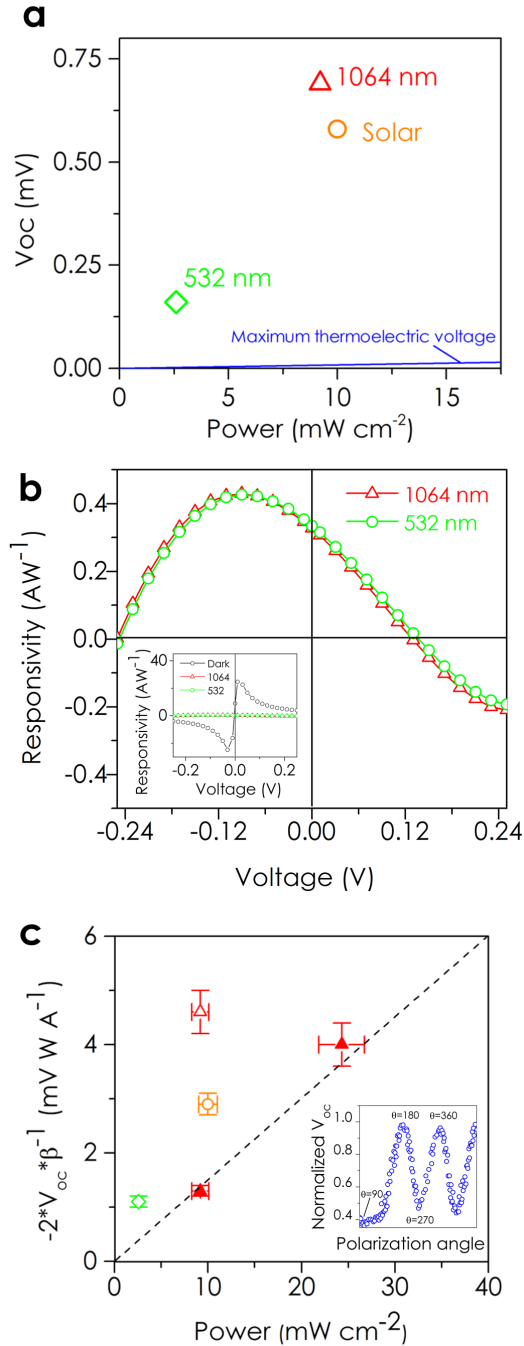
Figure 4| Optical rectification voltage and device responsivity. a, Measured open circuit voltage from 1.5 AM solar, 1064 nm, and 532 nm illumination versus the illumination power absorbed in the MWCNT rectenna device, which is 10% of the incident power based on the measured transmissivity of the semi-transparent top metal contact. The blue line is the maximum possible thermoelectric voltage for the same device structures under at least 112 times higher illumination intensity. **b,** Diode responsivity under 1064 nm and 532 nm illumination. The inset compares the illuminated and dark responsivity. **c**, The rectified voltage normalized by responsivity versus the illumination power absorbed in the MWCNT rectenna device. The open markers are from the devices in Fig. 3 and the closed markers are for a device from a different batch of MWCNTs with higher diode resistances. The inset shows the polarization dependence of the rectified voltage.

14

A Carbon Nanotube Optical Rectenna

Asha Sharma[‡], Virendra Singh[‡], Thomas L. Bougher[‡], and Baratunde A. Cola[*]

[*]Correspondence to: cola@gatech.edu
[‡]These authors contributed equally

This PDF file contains the methods with supplementary figures S1-S13 and supplementary tables S1-S2.

**S1. Turn-on voltage, field enhancement, effective barrier thickness, and asymmetry**

Two different metal electrodes with different work functions were tested to correlate the effect of metal work function on rectification ratio and turn-on voltage. Several multiwall carbon nanotube-insulator-metal (MWCNT-I-M) devices were fabricated in the same batch to produce similar array heights. These arrays were then coated with 8 nm of Al_2O_3 in the same atomic layer deposition (ALD) run. The turn-on voltage of MWCNT-I-M devices with Ca (work function ~ 2.9 eV) and Al (work function ~ 4.3 eV) top metal electrodes was determined based on the experimental current-voltage curves. The turn-on voltage was defined as the voltage at which a line fit to a linear portion of the current-voltage curve intercepts the y-axis (i.e., zero current, which is chosen to be 1 μA). This choice in definition of the turn-on voltage is arbitrary, so the main purpose of this analysis to create a self-consistent picture in which to compare the effects of work function on the onset of significant nonlinearity in our devices, and to estimate the extent of insulator barrier thinning due to geometric field enhancement. Figure S1 shows that the estimated turn-on voltage is 1.3 V smaller for Ca (0.3 V) top contact compared to Al (1.6 V).
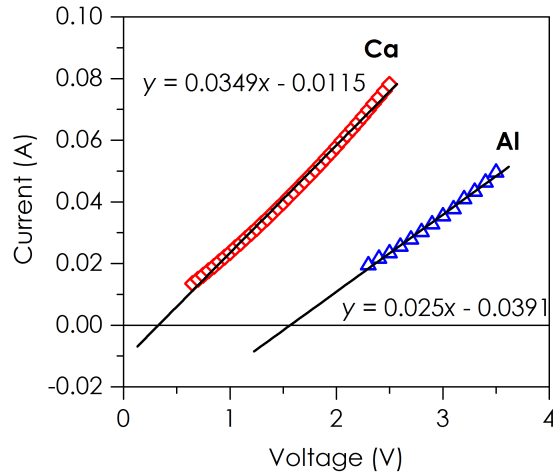
Supplementary Fig. S1. Determination of turn-on voltage from a linear portion of the measured current-voltage curves for MWCNT-I-Ca and MWCNT-I-Al devices.

To determine the effects of geometric field enhancement at MWCNT tips on diode rectification and turn-on voltage, we tested planar Au-Al_2O_3-Ca diodes, which were fabricated to closely match the contrast in work function and oxide thickness in the MWCNT-I-Ca devices for comparison. Planar M-I-M device geometries with glass/Ti/Au-Al_2O_3-Ca/Al were fabricated with various areas ranging from 0.01-0.04 cm^2 by first depositing Ti (30 nm)/Au (100 nm) on ultra-smooth glass substrates using e-beam evaporation. Then 8 nm of Al_2O_3 dielectric was deposited using ALD. Current-voltage characteristics measured on the planar devices with different active areas are shown in Fig. S2. The planar devices produced rectification ratios (~ 1.2 at ± 2.75 V d.c. bias) and tunnel currents (~ 1.5 μA/cm^2 at 2.75 V) that are several orders of magnitude lower than the currents produced in the MWCNT-I-Ca diodes (Fig. 2b). These results suggests that reduced effective barrier resistance due to geometric field enhancement could

contribute significantly to the much higher tunnel currents and asymmetry achieved in the MWCNT-I-M diodes. A simple energy level diagram is shown in Fig. 2a to illustrate the potential effects of work function contrast and field enhancement on the resistance to electron tunneling in MWCNT-I-M devices. Since the field enhancement is only expected in the forward direction, it contributes to unidirectional thinning of the tunneling barrier. This is because a single diode can be viewed roughly as a MWCNT point contact emitter against a planar surface (Fig. 1a).
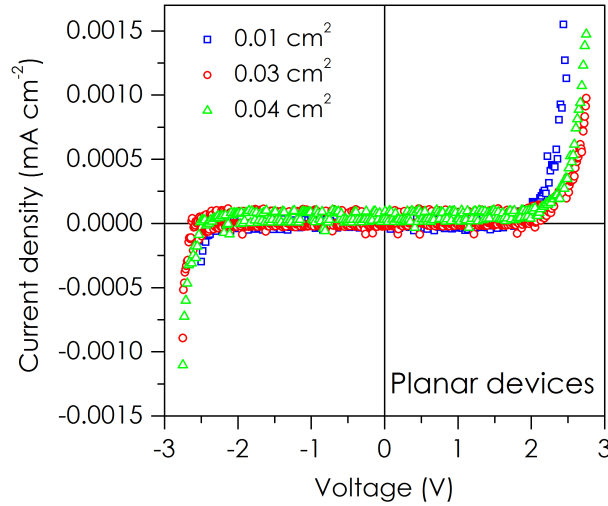
Supplementary Fig. S2. Current-voltage characteristics of planar M-I-M devices with glass/Ti/Au-Al$_2$O$_3$-Ca/Al structure with an active area of 0.01 cm^2, 0.03 cm^2, and 0.04 cm^2.

The electron tunneling equations from Simmons[1] are often used to fit experimental data for M-I-M diodes, however it has been shown that while these equations predict the behavior of planar structures qualitatively, the current density is often under-predicted significantly.[2,3] The current-voltage curves of CNT devices often differs somewhat from the exponential relationship between current and voltage in previous studies,[4] which is consistent with the observation in the MWCNT device data in this work. Understanding the limitations of this theory, the Simmons equations were used with the experimentally estimated turn-on voltages to determine the effective barrier thickness of an equivalent planar structure that would produce a current at these voltages. More recent work has developed numerical solutions to electron tunneling through insulators,[5-7] however the original analytical expressions using the WKB approximation are sufficient to examine the qualitative current-voltage behavior of planar devices.[8] The equivalent planar structures were used because CNT diode data does not fit well to classic tunneling theory because of effects including variation of curvature and electron density of states at CNT tips.[9,10] The equation for the current density under a forward applied bias for dissimilar electrodes separated by a dielectric barrier is given by Simmons:[11]

$$J = J_o \left\{ \overline{\varphi} \exp\left(-A\overline{\varphi}^{\frac{1}{2}}\right) - \left(\overline{\varphi} + eV\right) \exp\left[-A\left(\overline{\varphi} + eV\right)^{\frac{1}{2}}\right] \right\}$$

(1)

where, $J_o = \dfrac{e}{2\pi h \Delta s^2}$, and $A = \dfrac{4\pi \Delta s \sqrt{2m}}{h}$, $\overline{\varphi}$ is the average potential barrier height with respect to electrode Fermi level, V is the applied voltage, Δs is the barrier thickness, m is electron mass, h is Plank's constant, and e is the electronic charge.[11] When the image force potential is considered the effective work function is given as:

$$\overline{\varphi} = \varphi_2 - \left[\frac{s_1 + s_2}{2s}(eV + \Delta\varphi) \right] - \frac{1.15\lambda s}{\Delta s} \ln\left[\frac{s_2(s - s_1)}{s_1(s - s_2)} \right] \tag{2}$$

Where λ and s_1 are given by:

$$\lambda = \frac{e^2 \ln 2}{16\pi \varepsilon \varepsilon_o s} \tag{3}$$

$$s_1 = 1.2\lambda s / \varphi_2 \tag{4}$$

It should be noted that the expression for λ used here is a factor of 2 smaller than the original Simmons equation, which was in error as noted by Miskovsky et al.[7] For intermediate voltages $(eV > \varphi_1)$ s_2 is:

$$s_2 = s - \frac{9.2\lambda s}{3\varphi_2 + 4\lambda - 2(eV + \Delta\varphi)} + s_1 \tag{5}$$

and for high voltages $(eV > \varphi_1)$:

$$s_2 = \frac{(\varphi_2 - 5.6\lambda)s}{eV + \Delta\varphi} \tag{6}$$

ε is the dielectric constant of the insulator, and its value is taken to be 5.1 as determined from the measured capacitance values for 8 nm thin ALD deposited Al_2O_3 barrier on planar surface (see section S3 below). s is the barrier thickness and $\Delta s = s_2 - s_1$ and $\Delta\varphi = \varphi_2 - \varphi_1$. The barrier height at the metallic electrode is the difference between the electrode work function and the electron affinity of the oxide barrier. The barrier height, $\varphi_1 = 1.9$ eV for Ca, $\varphi_1 = 3.3$ eV for Al, and $\varphi_2 = 4.1$ eV for MWCNT was taken in the above expressions. All parameters in the current density equation were held constant except for the barrier thickness. A threshold current of 1 µA was set and the effective barrier thickness that would produce the threshold current was calculated. The area used for the current calculation was the projected device area (0.01 cm^2) multiplied by the fill fraction of the MWCNTs (0.005) for an effective area of 5×10^{-5} cm^2. Because the two devices were identical except for the work function of the metal electrode, it was expected that the difference between the work function of Ca and Al could account for the difference in turn-on voltages that was observed experimentally. Since the deposited barrier thickness was the same in both devices, it is expected that the modeled effective barrier thickness of each device would also be the same. The physical barrier thickness of the device is 8 nm, but this does not account for the electron tunneling enhancement produced by the concentrated electric field at the tips of the MWCNTs. The effective electron tunneling barrier thickness (s_{eff}) was determined to be approximately 1.5 nm for both Ca and Al. These are the barrier thickness in a planar device that would produce 1 µA of current at the respective turn-on voltages. A plot of the theoretical current-voltage for Ca and Al planar devices with the aforementioned barrier thickness are shown in Fig. S3. This result provided confirmation that the difference in work function of the two top metals was responsible for the change in turn-on voltage between the two device types.
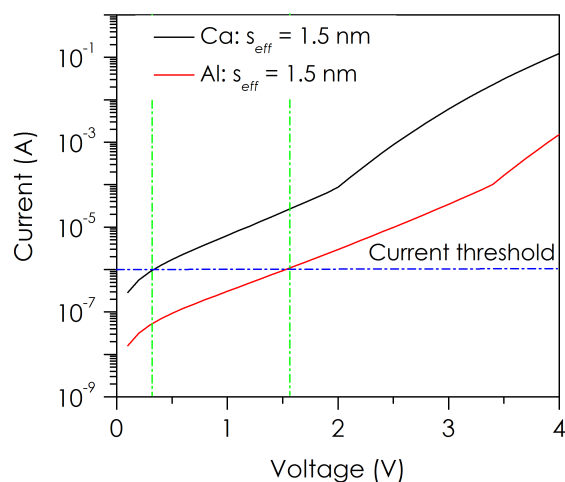
Supplementary Fig. S3. Theoretical current-voltage characteristics and estimated effective barrier thicknesses (s_{eff}) based on an equivalent planar MWCNT-I-Ca and MWCNT-I-Al structures (i.e., the same material properties were used) that would produce a magnitude of current similar to experimentally observed currents at the turn-on voltages (0.3 and 1.6 V for Ca and Al, respectively). The arbitrary current threshold that defines voltage turn on is 1 μA.

The current-voltage curves for the planar devices (Au-Al$_2$O$_3$-Ca) were fitted using the above Simmons' theoretical electron tunneling equations by fitting for the effective barrier thickness, s_{eff}. This application of Simmons' equations is also similar to previous work that changed the barrier thickness to fit the model.[8] The data and best-fit theoretical curves are shown in Fig. S4 with the experimentally measured data. It can be seen that the theoretical fittings agree well with the measured current-voltage curves for three different devices. The s_{eff} in the planar Au-Al$_2$O$_3$-Ca diodes is estimated to be 2.8 nm from fitting Simmons' theory to three devices with different areas (0.01 cm^2, 0.03 cm^2, 0.04 cm^2) as shown in Fig. S4. The Au and Al$_2$O$_3$ layers were measured with atomic force microscopy to be atomically smooth (rms roughness of 0.52 ± 0.06 and 0.64 ± 0.02 nm, respectively); therefore, it is unlikely that surface roughness contributes to field enhancement in the planar diodes, as has been observed in prior work.[8] The fact that the effective barrier thickness is thinner than the physical barrier thickness means that the tunneling equations under predict the current density, which is consistent with previous findings.[8,12] The nearly twofold reduction in s_{eff} for MWCNT-I-M diodes compared to the equivalent planar structures presents strong evidence that field enhancement at MWCNT tips contributes to effective barrier thinning in these devices. However, the effective device field enhancement is expected to be less than that of a single CNT because of collective screening of the external field by neighboring tubes in the array.[13]
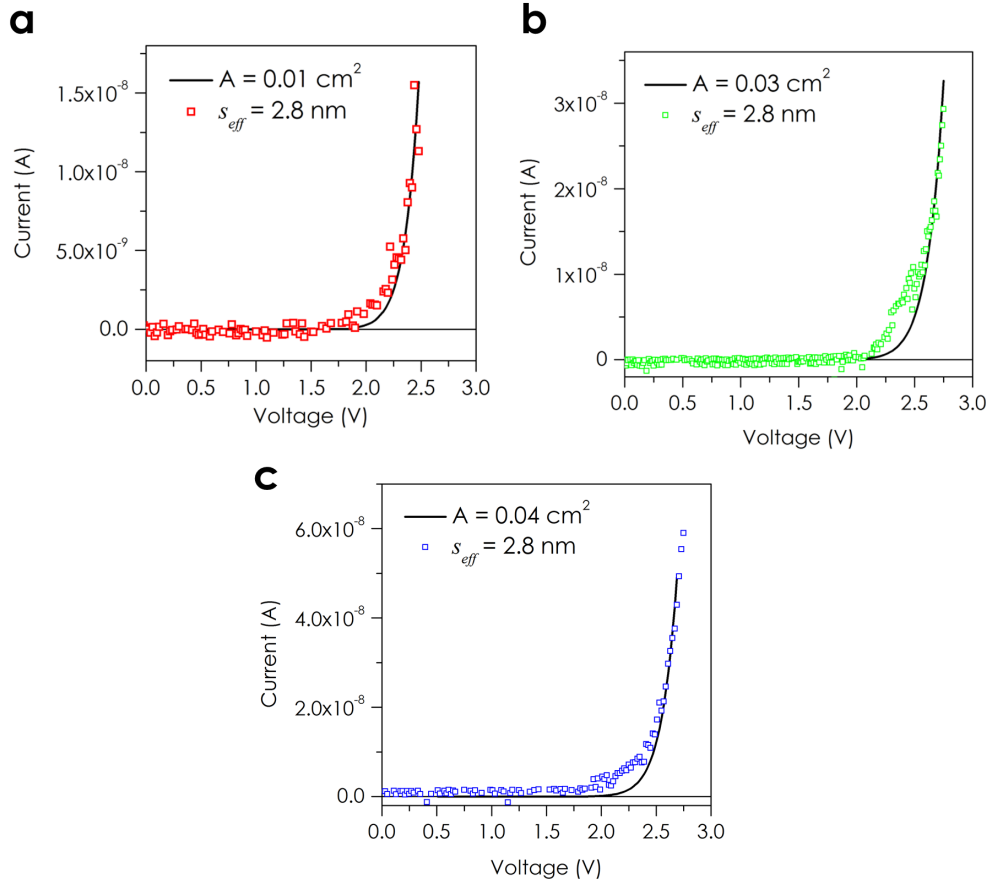
Supplementary Fig. S4. The fitted curves and experimental data for three different planar devices with different active area, (a) 0.01 cm^2, (b) 0.02 cm^2, (c) 0.04 cm^2.
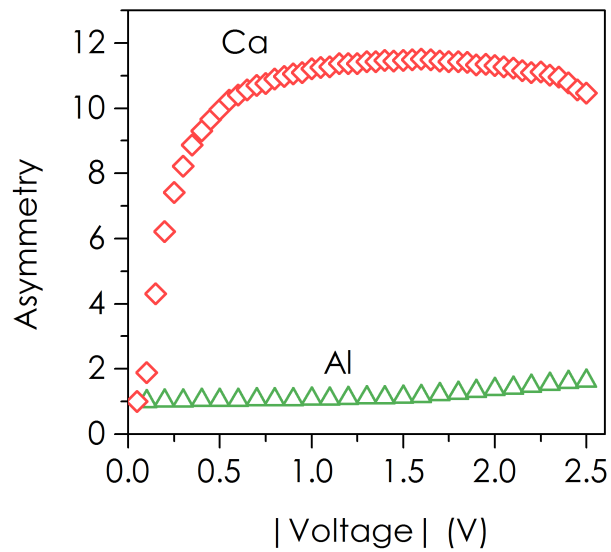

Supplementary Fig. S5. Electrical asymmetry (A) of Ca and Al devices in Fig. 2b where $A = |I(V)/I(-V)|$.

S2. Effect of MWCNT work function on electrical performance

Different CNT growth conditions or substrates can produce MWCNT structures with different morphology and can result in different electrical properties and work functions.[14] The work functions of MWCNTs grown on Si substrates with different resistivities were measured by Kelvin probe on three different spots on the same sample and on MWCNTs grown in different batches (Fig. S6a). The MWCNTs that were grown on medium resistivity Si substrates (0.01-0.05 Ω.cm) exhibited a higher work function (5 eV) than the work function of MWCNTs that were grown on low resistivity Si (0.001-0.005 Ω.cm), which was 4.8 eV. The MWCNTs with 5 eV work function were used in the devices in the main text.

In order to correlate the diode current rectification with the bottom MWCNT electrode work function, Al_2O_3 was deposited on the two MWCNT samples followed by the deposition of a Ca top metal electrode. The inset in Fig. S6a indicates clearly that the rectification in the current for a given applied dc bias is higher in devices that use MWCNTs with a higher work function. These results were reproducible on several devices as shown in Fig. S6. Evaluation of the samples in scanning electron microscope (SEM) revealed that the MWCNTs that were grown on low resistivity substrates were less straight in comparison to the MWCNTs that were grown on medium resistivity substrates (Fig. S6b and S6c). The higher degree of CNT waviness could explain the lower work functions measured on the MWCNTs grown on low resistivity Si substrates because such waviness could increase defects, entanglement, and as a result cause a substantial decrease in the electrical conductivity of the MWCNTs.[15]
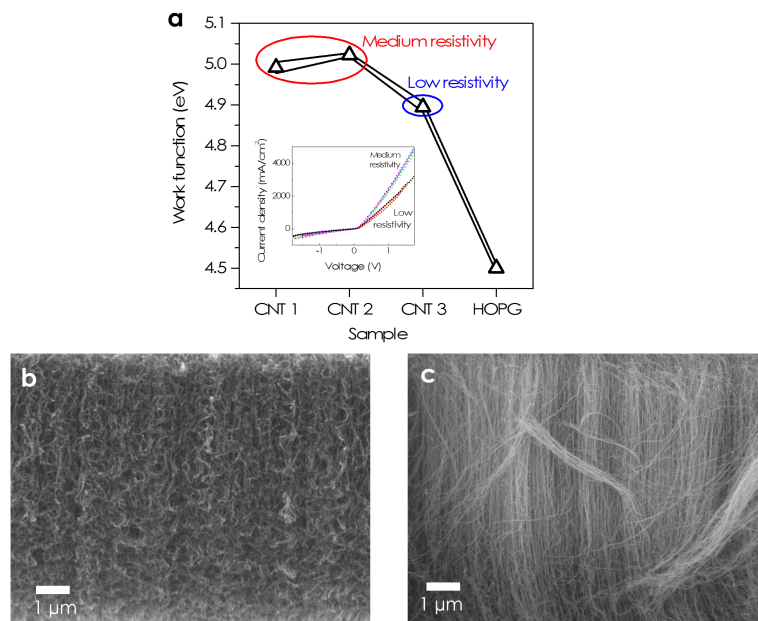
Supplementary Fig. S6. Effect of MWCNT work function on current-voltage characteristics. (a) work function of the MWCNTs grown on medium resistivity and low resistivity Si substrates. The inset shows current-voltage characteristics of the devices fabricated using the low work function (WF), and high WF MWCNTs as the bottom electrode in the diode structure. (b) SEM image of MWCNT arrays on low resistivity (0.001-0.005 Ω.cm) Si substrate. (c) SEM image of MWCNT arrays on medium resistivity (0.01-0.05 Ω.cm) Si substrate.

S3. Capacitance measurements of MWCNT-O-M diode arrays

The measured capacitances (C) based on the apparent device area (0.1 cm^2) of MWCNT-I-M diode arrays with different oxide thicknesses (Fig. 2c) were nearly constant in a standard low frequency range (up to 10^6 Hz). The results do not show the inverse thickness relation of a conventional parallel plate capacitor because the permittivity of nanoscale oxide insulators can decrease with thickness.[16] For the MWCNT-O-M arrays fabricated with 8 nm Al$_2$O$_3$, specific capacitance of approximately 3.4 µF/cm^2 or roughly 2 attofarads per MWCNT junction, and a dielectric constant (ε) of 3.8 can be extracted using the following expression

$$C = C_1 + C_2 + C_3 \text{............} = n\left(\frac{\varepsilon_0 \varepsilon A}{d}\right).$$
(7)

The measured capacitance is 1.7 nF for an 8 nm oxide (Fig. 2c). The measured MWCNT diameter is approximately 8 nm, so the area of a MWCNT tip $= \pi \times 4^2 \times 10^{-14}$ cm^2 = 50.24 $\times 10^{-14}$ cm^2. Based on the number density of MWCNTs estimated from SEM images, there are approximately 10^9 MWCNTs in an area of 0.1 cm^2. Therefore, the actual area A = 50.24 $\times 10^{-14}$ cm^2 $\times 10^9$ = 50.24 $\times 10^{-5}$ cm^2. Hence, the specific capacitance C/A = 1.75 nF/50.24 $\times 10^{-5}$ cm^2 = 0.0338 $\times 10^{-4}$ F/cm^2 = 3.38 $\times 10^{-6}$ F/cm^2 = 3.38 µF/cm^2. The dielectric constant (ε) of 3.8 can be extracted from the calculated specific capacitance for 8 nm oxide by using the equation,

$$\varepsilon = \left(C/A\right) \times \frac{d}{\varepsilon_0}.$$
(8)

Similarly, the capacitance per junction can be evaluated by dividing the measured capacitance (1.7 nF) by the number of MWCNTs in an area of 0.1 cm^2 (10^9 MWCNT). Hence, the capacitance per junction is 1.7 nF/10^9, which is 1.7 $\times 10^{-18}$ F.

The measured capacitances (at 1 kHz and 20 mV$_{rms}$) of the planar Au-Al$_2$O$_3$-Ca devices with 8 nm of oxide as a function of area (ranging from 0.01-0.04 cm^2) are shown in Fig. S7. The capacitance per unit area (C/A) as extracted from the linear fit of the slope of capacitance versus area curve is 569 nF/cm^2. Using the value of C/A in a conventional parallel plate capacitor model where capacitance is given by equation (8), a dielectric constant (ε) of 5.14 is calculated for the ALD deposited 8 nm Al$_2$O$_3$.
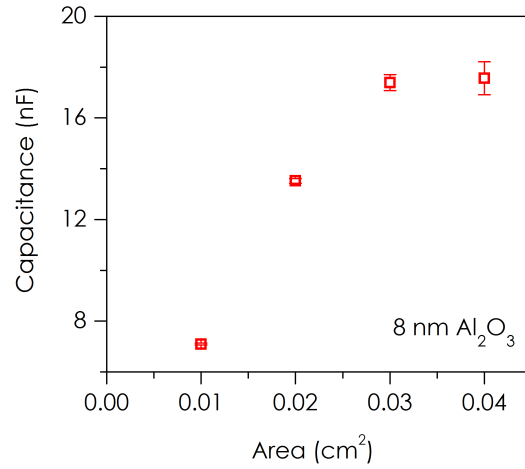
Supplementary Fig. S7. Measured capacitance of planar Au-Al_2O_3-Ca (8 nm oxide) structures as a function of area, at 1 kHz and ac amplitude of 20 mV_{rms}.

**S4. Device consistency and reliability**
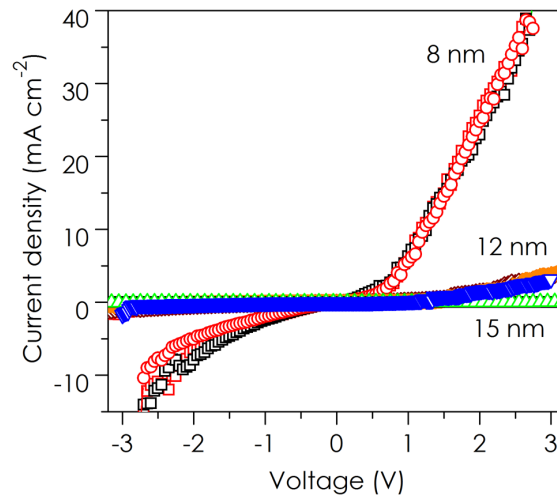
Supplementary Fig. S8. Carbon nanotube-insulator-metal tunnel diode characteristics. The current-voltage characteristics of the tunnel diodes using 8, 12, and 15 nm of Al_2O_3. Multiple repeat scans are shown for each data set to demonstrate consistency.
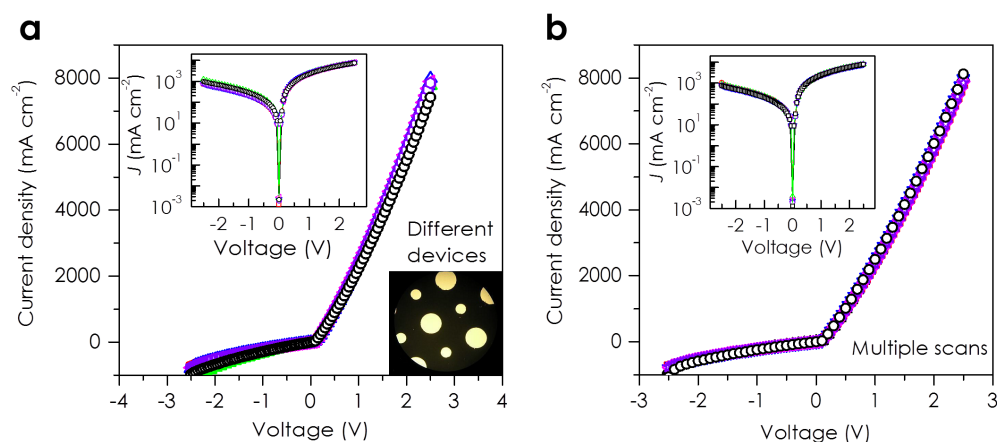
Supplementary Fig. S9. (a) Current-voltage characteristics of the fabricated MWCNT-I-Ca diodes measured on six devices with an active area of 0.01 cm^2 (the picture shows an optical image of the devices with two different top contact areas). (b) current-voltage characteristics of a device showing excellent electrical stability during multiple scans. The insets in (a) and (b) show semi-logarithmic plots of the data.

S5. Optical rectification photoresponse of devices in Fig. 3
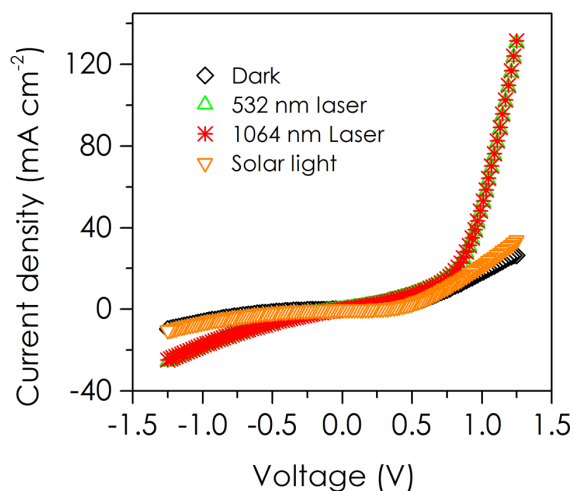
Supplementary Fig. S10. Optical rectification of infrared, visible, and simulated solar light. **a**, Current-voltage characteristics of device responding to 1.5 AM solar (100 mW cm^{-2}), 1064 nm (92 mW cm^{-2}), and 532 nm (26 mW cm^{-2}) illumination with 10% transmission through the top metal contact.

Supplementary Table S1. Dark and illuminated diode characteristics, measured open-circuit voltage and short-circuit current, and estimated energy conversion efficiencies for the devices in Fig. 3 of the main text. The statistical uncertainty in the extracted diode characteristics is approximately ±10% and approximately ±5% in the measured voltage and current. The illuminated diode resistance and responsivity are based on applying a classical treatment to the illuminated $I(V_{dc})$ curve – the illuminated $I(V_{dc})$ curve is shifted in this case such that $I = 0$ at $V_{dc} = 0$. While this approach is only an approximation, it is useful when the range of voltages tested for dark $I(V_{dc})$ characteristics is less than $\pm\hbar\omega$, and we find the agreement with equations (1) and (2) at $V_{dc} = 0$ to be within ±30%.

| Device	Dark		Illuminated		Measured V_{oc} (mV)	Measured I_{sc} (mA cm^{-2})	Estimated conversion efficiency (%)
	Zero bias resistance (kohm cm²)	Zero bias responsivity (V^{-1})	Zero bias resistance (kohm cm²)	Zero bias responsivity (V^{-1})			
1064 nm laser (Figure 3b)	7.5	9	0.08	0.3	-0.69	$6.5*10^{-3}$	10^{-5}
532 nm laser (Figure 3c)	7.5	9	0.07	0.3	-0.16	$1.7*10^{-3}$	$3*10^{-6}$
AM 1.5 solar (Figure 3d)	5.1	4.1	5.7	0.4	-0.58	$3.0*10^{-4}$	$4*10^{-7}$
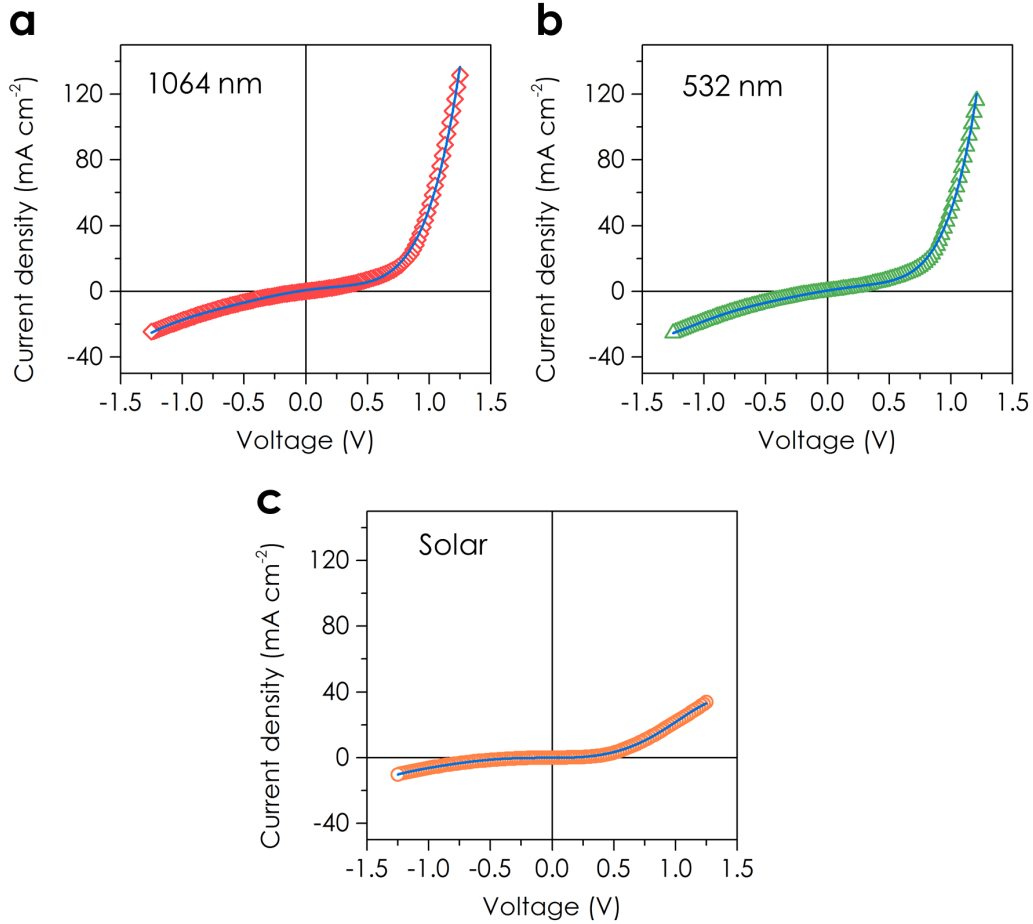
Supplementary Fig. S11. Illuminated current-voltage response, corrected such that $I = 0$ at $V_{dc} = 0$, for (a) 1064 nm, (b) 532 nm, and (c) 1.5 AM solar illumination. These are the same devices as those in Fig. 3. The black curve is a 6th-order polynomial fit to the data that is used to compute the differential resistance and responsivity as an approximation to the semi-classical response.

Supplementary Table S2. Comparison to previous reports of optical rectification in metal-vacuum-metal (MVM) junctions. Results from this work reported for 532 nm light with 8 nm oxide device with Ca top metal.

Authors	Year	Pressure	Junction	Max Current at Zero Bias (A)	Incident Power (W/cm²)	Ratio Current to Laser Intensity (A-cm²/W)
Nguyen et. al.[18]	1989	Vacuum	MVM	2.0E-09	20	1.00E-10
Miskovsky et. al.[7]	2010	Vacuum	MVM	1.0E-13	0.13	7.85E-13
Ward et. al.[19]	2010	Vacuum	MVM	9.0E-09	22600	3.98E-13
Bragas et. al.[20]	1998	Vacuum	MVM	3.0E-12	30	1.00E-13
This work	2015	1 atm	MIM	1.0E-05	0.092	1.09E-04

S6. Thermoelectric response
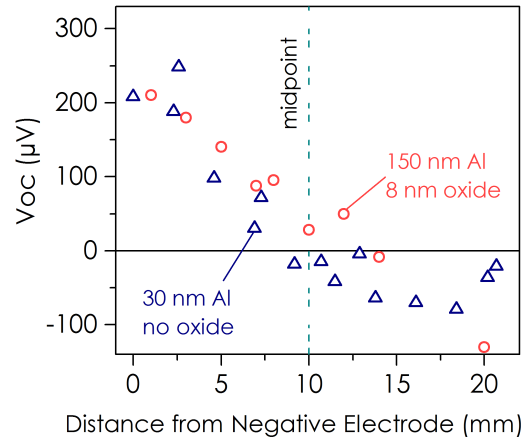
Supplementary Fig. S12. Thermoelectric voltage vs. distance from the negative probe for a typical MWCNT-I-M rectenna with 150 nm Al capping layer to absorb all thermal energy at the surface. The sample is heated at 11.2 W/cm^2 532 nm laser intensity, which is about 112 times more intense than the maximum illumination intensity in our rectenna response tests. Also shown is a device with a semi-transparent 30 nm top Al metal and no oxide layer. The red dashed line is the background voltage level. The halfway point between the positive and negative probe is approximately 10 μm from the negative probe.

S7. Additional evidence for optical rectification
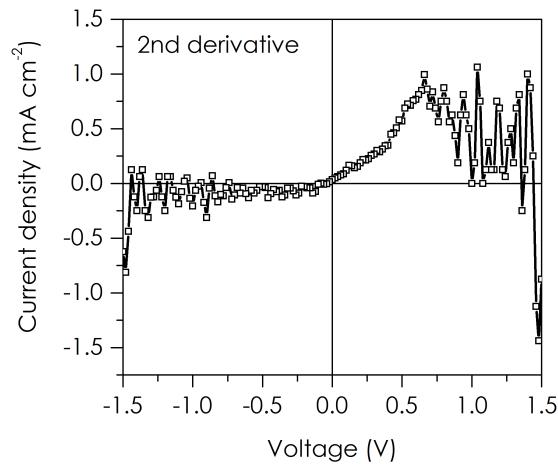
Supplementary Fig. S13. MWCNT rectenna device under 1.5 AM solar illumination. The 2nd derivative is computed from a 6th-order polynomial fit to the illuminated current-voltage curve (from Fig. S11c) to approximate the semi-classical correction. The agreement in the shape and sign of the voltage where the 2nd derivative of the current-voltage crosses the abscissa with the data in Fig. S11c is evidence for the photoresponse originating from optical rectification.[17]

References

1   Castrucci, P. *et al.* Light harvesting with multiwall carbon nanotube/silicon heterojunctions. *Nanotechnology* **22**, 115701 (2011).
2   Park, B., Kim, Y. J., Graham, S. & Reichmanis, E. Change in Electronic States in the Accumulation Layer at Interfaces in a Poly(3-hexylthiophene) Field-Effect Transistor and the Impact of Encapsulation. *ACS Applied Materials & Interfaces* **3**, 3545-3551 (2011).
3   Luo, J., Zhu, J., Huang, Z. & Zhang, L. Arrays of Ni nanowire/multiwalled carbon nanotube/amorphous carbon nanotube heterojunctions containing Schottky contacts. *Appl. Phys. Lett.* **90**, 033114 (2007).
4   Xiao, K. *et al.* Photoelectrical characteristics of a C/CNx multiwalled nanotube. *Adv. Func. Mater.* **17**, 2842-2846 (2007).
5   Ghatak, A. K., Thyagarajan, K. & Shenoy, M. R. Novel numerical technique for solving the one-dimensional Schroedinger equation using matrix approach - application to quantum well structures. *IEEE Journal of Quantum Electronics* **24**, 1524-1531 (1988).
6   Hashem, I. E., Rafat, N. H. & Soliman, E. A. Theoretical study of metal-insulator-metal tunneling diode figures of merit. *IEEE Journal of Quantum Electronics* **49**, 72-79 (2013).
7   Miskovsky, N. M., Cutler, P. H., Feuchtwang, T. E. & Lucas, A. A. The multiple-image interactions and the mean-barrier approximation in MOM and MVM tunneling junctions. *Appl. Phys. A* **27**, 139-147 (1982).
8   Cowell, E. W. *et al.* Advancing MIM electronics: amorphous metal electrodes. *Adv. Mater.* **23**, 74-78 (2011).
9   Buldum, A. & Lu, J. P. Electron Field Emission Properties of Closed Carbon Nanotubes. *Phys. Rev. Lett.* **91**, 236801 (2003).
10   Bonard, J.-M., Kind, H., Stockli, T. & Nilsson, L.-O. Field emission from carbon nanotubes: The first five years. *Solid-State Electronics* **45**, 893-914 (2001).
11   Simmons, J. G. Electric tunnel effect between dissimilar electrodes separated by a thin insulating film. *J. Appl. Phys.* **34**, 2581-2590 (1963).
12   Krishnan, S., Stefanakos, E. & Bhansali, S. Effects of dielectric thickness and contact area on current–voltage characteristics of thin film metal–insulator–metal diodes. *Thin Solid Films* **516**, 2244-2250 (2008).
13   Mayer, A., Miskovsky, N. M., Cutler, P. H. & Lambin, P. Transfer-matrix simulations of field emission from bundles of open and closed (5,5) carbon nanotubes. *Phys. Rev. B* **68**, 235401 (2003).
14   Su, W. S., Leung, T. C., Bin, L. & Chan, C. T. Work function of small radius carbon nanotubes and their bundles. *Appl. Phys. Lett.* **90**, 163103-163101 (2007).
15   Dai, H. J., Wong, E. W. & Lieber, C. M. Probing electrical transport in nanomaterials: Conductivity of individual carbon nanotubes. *Science* **272**, 523-526 (1996).
16   de Jonge, N., Lamy, Y., Schoots, K. & Oosterkamp, T. H. High brightness electron beam from a multi-walled carbon nanotube. *Nature* **420**, 393-395 (2002).
17   Ward, D. R., Huser, F., Pauly, F., Cuevas, J. C. & Natelson, D. Optical rectification and field enhancement in a plasmonic nanogap. *Nat. Nanotech.* **5**, 732-736, (2010).
18   Nguyen, H. Q. *et al.* Mechanisms of Current Rectification in an Stm Tunnel Junction and the Measurement of an Operational Tunneling Time. *IEEE Trans. Electron Dev.* **36**, 2671-2678 (1989).
19   Ward, D. R., Huser, F., Pauly, F., Cuevas, J. C. & Natelson, D. Optical rectification and field enhancement in a plasmonic nanogap. *Nat. Nanotech.* **5**, 732-736, (2010).
20   Bragas, A. V., Landi, S. M. & Martinez, O. E. Laser field enhancement at the scanning tunneling microscope junction measured by optical rectification. *Appl. Phys. Lett.* **72**, 2075-2077 (1998).